JOURNAL OF MATERIALS SCIENCE 32 (1997) 921–930

Damage of 6061/SiC_w composite by thermal cycling

C. BADINI
Dipartimento Scienza dei Materiali e Ingegneria Chimica, Politecnico di Torino, Italy

M. LA VECCHIA
Dip. di Meccanica, Università di Brescia, Italy

A. GIURCANU
Institute für Werksloffkunde, Technische Hochschule Darnstadt, Germany

J. WENHUI
Department of Metal Materials Engineering, Shenyang Polytechnic University, China

The unreinforced 6061 alloy and a 6061/SiC composite, at the beginning in the T6 temper, were submitted to thermal cycling (up to 2000 cycles) in the temperature ranges 25–180 °C and 25–220 °C. The microstructure of these materials was studied by scanning electron microscopy and mercury intrusion porosimetry. Mechanical and thermomechanical properties were also investigated. Tensile strength, hardness, Charpy impact resistance, fracture toughness, density, specimen dimensions and thermal expansion were compared before and after thermal cycling. The unreinforced alloy showed an increase of ductility with cycling. This behaviour was chiefly due to overageing and partial annealing. The composite material, following the thermal treatment, did not only undergo overageing and annealing of its metal matrix; void coalescence, crack formation and reinforcement debonding were also observed. The development of these defects basically resulted in a marked decrease of tensile strength, yield strength, Charpy impact energy and fracture toughness.

1. Introduction

Metal matrix composites (MMCs) have been widely studied in recent years as materials of great interest for structural applications. These composites offer increased specific strength and stiffness over monolithic materials, in particular in severe environments. For this reason, they are most widely used for structural parts operating at high temperature. Long-fibre MMCs with matrices of titanium alloys or of intermetallics, can be employed in aircraft at elevated temperatures. Furthermore MMCs reinforced by particulates or whiskers can work at high temperature, for instance, when used as partly reinforced pistons for diesel engines.

MMCs are not only submitted to thermal exposure in service, but generally also experience rapid temperature changes during processing. Owing to the appreciable difference in the thermal expansion coefficient between reinforcement and metal matrix, internal stresses and a high dislocation density (near the metal matrix/ceramic interface) are generated following these temperature changes [1, 2]. Diffraction techniques were used to measure the residual stresses [3, 4]. The high dislocation concentration was observed by transmission electron microscope and it was believed to strengthen the material. Furthermore, MMCs will probably undergo thermal cycling in service and suffer compression–tension fatigue. Composites could be degraded by thermal fatigue, depending on the heating and cooling rates and the characteristics of their constituents. During thermal cycling, new internal stresses can be generated and stress relief phenomena can occur. These last phenomena involve generation of dislocation, but, simultaneously, a process of reorganization or annihilation [5–7] of dislocations generally occurs. The density of dislocations would increase or decrease depending on whether the generation or annihilation process prevails [6, 8]. Anyway, the internal stresses can lead to plastic yielding of the matrix when the elastic stress exceeds the matrix yield stress.

Analyses of elastic–plastic behaviour of composites during thermal cycling have been performed and relative theoretical models have been proposed by several authors [9–15]. Some of these theoretical models do not take into account the reinforcement morphology [9, 15], while others refer to a particular shape of the reinforcement: long fibres [10–12], whiskers [13], particles [14]. In spite of this, the comparison of some of these models [9–12] showed that they give very similar outcomes [16].

The internal stresses were also recognized as being responsible for the superplasticity of metal matrix composites, as they can assist the matrix plastic flow in the direction of a low external load applied during thermal cycling [8, 17–21]. The models in the literature account for the residual stresses and the plastic deformations measured in several thermally cycled composites. However, experimental results showed that other kinds of composite damage also occurred,

0022–2461

depending on the shape of the reinforcement and the characteristics of the metal/ceramic interface as well. Thermal cycling of long-fibre composites chiefly results in the plastic flow of the matrix and in a consequent dimensional change of samples: extension of the matrix along the reinforcing fibres and shrinkage in the transverse direction [12, 22, 23]. However, interfacial reactions between matrix and fibres can occur during cycling, giving rise to the formation of brittle interfacial layers which are prone to undergo cracking [24–28].

The influence of this kind of composite modification on the mechanical properties has not been well assessed. For instance, after thermal cycling of titanium/SCS6 composite, carried out with a large temperature change, the material tensile strength greatly decreased according to some authors [26, 28], while others found it was practically unchanged [24, 25]. When the fibre/matrix interfacial bond is not strong enough (for instance in the case of Al_2O_3 fibres coupled with a superalloy or an intermetallic matrix [29, 30]) thermal cycling causes fibre debonding instead of cracks in the matrix.

In the case of other fibre-reinforced composites, an increase of specimen surface roughness [6] or the formation of porosity at the matrix/fibre interface [31] were also observed following thermal cycling. The thermal cycling response of composites reinforced by long fibres has been widely investigated, while relatively little research has been reported about the thermal fatigue of aluminium or magnesium-based composites containing particles or whiskers [19, 21, 32–35]. Dilatometric experiments showed that this last class of composites can also undergo a net elongation parallel to the direction of whisker alignment during thermal cycling [33]. In fact, according to some authors [19, 21, 32, 34] prolonged cycling (up to 1000 cycles), carried out between room temperature and 400–500 °C without an applied external load, can result in a material plastic deformation ranging between 5% and 15%. After these treatments a large decrease of both ultimate tensile strength and yield strength was observed and attributed to thermal fatigue [32, 35] or to matrix overageing [34].

Literature data do not agree about the effect of cycling on composite elastic modulus, which was observed to be unchanged [32, 34] or appreciably lowered [35] after thermal treatment. Only a few data were reported about the influence of thermal fatigue on composite toughness [35]. According to some authors [21, 34] neither cavitation nor debonding occur during cycling, even though the formation of voids was also occasionally found [35]. Most of the reports in the literature refer to thermal cycling carried out from room temperature up to 400–500 °C. The upper temperature limit used in these experiments would be appreciably higher than that reached by aluminium/SiC composites in service. In fact, it should be taken into account that both the tensile and the yield strength of these materials even at 350 °C are only about 50% of those shown at room temperature [36]. In this work the composite was submitted to less severe cycling conditions, in order to simulate the thermal gradients that this material is likely to experience in service.

2. Experimental procedure

A composite of 6061 aluminium metal matrix reinforced by 20 vol% SiC whiskers was investigated. This composite was produced (Pechiney Aluminium) by squeeze casting of SiC preforms; a subsequent hot extrusion of the cast billets provided round bars of 20 mm diameter. Bars of 20 mm diameter of unreinforced 6061 alloy, fabricated by casting and hot extrusion, were used as a reference material. Both microstructure and mechanical properties of these two materials were investigated before and after thermal cycling. Dimensional stability, density, pore-size distribution, tensile properties, hardness, impact resistance, fracture toughness and thermal expansion coefficient, were tested.

All the specimens for mechanical tests and microstructure characterization were submitted to a prior T6 heat treatment. The solution treatment was carried out at 557 °C in a salt bath for 2 h; after quenching in a brine bath the specimens were aged at 180 °C until the maximum strength was achieved. Different ageing periods of 10 and 4 h were adopted for the unreinforced alloy and the composite, respectively, in order to take into account the different ageing rate of these two materials [37]. Afterwards, the specimens were submitted to rapid heatings and coolings in a thermal cycling apparatus especially built up for this purpose. An electrical motor was used to move, by means of a mechanical arm, the sample holder (a basket made of a metallic grate) from a bath at room temperature to another polysiloxanic oil bath kept at 180 or 220 °C. Thermal cycling was performed up to 2000 cycles; each cycle involved one heating and one cooling step. The specimens remained in each oil bath for 6 min then they were transferred into the other one.

The true temperature change experienced by the samples during one single cycle was measured by means of a digital thermometer. This measurement was carried out by keeping a thermocouple both on the sample surface and in a hole made along the sample axis. Fig. 1 shows the temperature variations on the

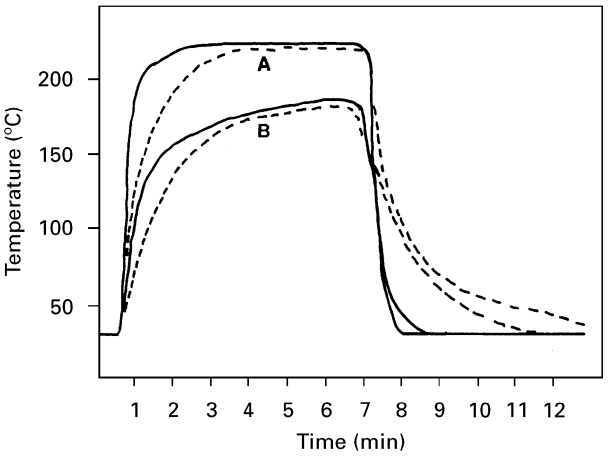

Figure 1 Temperature changes during a thermal cycle up to 220 °C (curves A) and up to 180 °C (curves B): (——) on the sample surface, (– – –) in the sample interior.

surface and in the core of the sample during the cyclings performed up to 180 and 220 °C. The temperature change was found to be practically identical for the composite and the unreinforced alloy despite their different compositions.

Round tensile specimens (120 mm long, 6.2 mm diameter at the reduced section) were machined in the longitudinal direction from the bars of the composite and the unreinforced alloy. As a consequence of the extrusion process, the whiskers were oriented along the axis of the bars and therefore they were aligned longitudinally in the tensile specimens also. Tensile tests were performed at room temperature at a constant crosshead speed of 0.3 mm min^{-1} by means of a Sintech 10D equipment; an extensometer was used to measure the axial strain. The 0.2% offset yield strength, σ_y, the ultimate tensile strength, UTS, the Young's modulus, E, and the elongation to failure, Δl, were measured. The morphology of the fracture surfaces was observed by scanning electron microscopy (SEM; Philips 525M).

Other samples for determination of Charpy impact resistance were taken longitudinally from the bars. Standard Charpy V specimens, 55 mm long and 10 mm thick, were used for the impact tests. The impact tests were performed by using an Izod–Charpy apparatus (ATS-FAAR), equipped with a hammer of 3.5 and 19.9 kg for the composite and the unreinforced alloy, respectively. The tests were instrumented to record the load–time curves. The 6061/SiC composite fracture toughness was also evaluated by means of fracture mechanics tests carried out at room temperature. Precracked Charpy V type specimens loaded in three-point bending were used to assess the fracture toughness according to ASTM E399 standard. The critical stress intensity factor, K_{Ic}, was calculated by means of a screw-driven 100 kN Instron machine at a crosshead speed of 0.1 mm min^{-1}.

Brinell hardness measurements were performed in the following experimental conditions: ball indentor diameter 2.5 mm, load 62.5 kg.

The length and the thickness of all the impact test specimens and the length and the diameter at the reduced section of the tensile samples were compared before and after the thermal cycling. The dimensional measurements were performed by an electronic digital caliper with a precision of 0.1 mm. The material density was determined from the ratio between the specimen weight (measured in air) and the buoyancy measured after immersion of the specimen in water. The water density at the laboratory temperature was considered in the density calculation.

Discs of material (diameter 15 mm, thickness 5 mm) were machined transversally from the bars and used for porosimetric measurements carried out by mercury intrusion (Fisons 2000 equipment). Mechanical tests were performed on at least three samples (five in the case of impact tests and porosimetric measurements) for each material and treatment condition, then the results were averaged.

The microstructure of the materials was observed by scanning electron microscopy on the transverse section of tensile specimens of both the T6 treated and the thermally cycled samples. The thermal expansion coefficient (CTE) of the materials was measured by dilatometry (Netzsch, Dil 402 equipment). Small bars (35 mm long and 8 mm diameter) were tested under an argon atmosphere with a scanning rate of 5 °C min^{-1}. The thermal expansion of the materials in the T6 temper was compared with that resulting from the following heat treatments: 2000 cycles performed up to 220 °C in the equipment described above, 20 cycles carried out in a furnance under an argon atmosphere between 25 and 500 °C (heating rate 100 °C min^{-1}).

3. Results and discussion

3.1. Dimensional stability

The dimensions of the specimens for impact tests and their densities measured before and after thermal cycling are compared in Table I. The average values of length and thickness are reported in the table with the standard deviation (σ_{n-1}) and the fractional standard deviation ($\sigma_{n-1}/\bar{X}$), used as indexes of experimental errors.

Table I shows that the slight differences in the average specimen dimensions measured before and after thermal cycling can probably be attributed to experimental errors. Any significant variation in both specimen length and thickness resulted from thermal

TABLE I Dimensional stability after thermal cycling of impact test specimens (L = length; T = thickness; d = density; σ_{n-1} = standard deviation $\times 10^{-1}$; $\sigma_{n-1}/\bar{X}$ = fractional standard deviation $\times 100$)

Sample	L (mm)	σ_{n-1}	$\sigma_{n-1}/\bar{X}$	T (mm)	σ_{n-1}	$\sigma_{n-1}/\bar{X}$	d (g cm^{-3})	σ_{n-1}	$\sigma_{n-1}/\bar{X}$
6061	55.02	0.37	0.067	10.06	0.27	0.268	2.721	0.24	0.871
6061 (2000 cycl. 180 °C)	55.02	0.33	0.060	10.08	0.35	0.347	2.703	0.05	0.172
6061 (2000 cycl. 220 °C)	55.02_5	0.40	0.073	10.04	0.21	0.209	2.714	0.01	0.022
6061/SiC	55.02	0.55	0.099	10.09	0.33	0.326	2.749	0.19	0.673
6061/SiC (2000 cycl. 180 °C)	55.02_5	0.61	0.110	10.06_5	0.28	0.278	2.750	0.09	0.331
6061/SiC (2000 cycl. 220 °C)	55.02	0.64	0.116	10.07	0.36	0.357	2.770	0.17	0.628

cycling of unreinforced 6061 alloy and 6061/SiC_w composite. The comparison of density values before and after thermal cycling (Table I) confirms that the specimens did not suffer appreciable volume change in the experimental conditions adopted. Daehn *et al.* [22] estimated the temperature variation needed to cause the matrix to deform plastically by two different equations which depend on the shape of the ceramic reinforcement of the composite. For a composite reinforced by long fibres

$$\Delta T = (1 + E_m V_m / E_f V_f)\,\varepsilon_0 / \Delta\alpha \quad (1)$$

In the case of composites containing ceramic particles

$$\frac{\Delta\alpha\,\Delta T}{\varepsilon_0} = \frac{1 - v_m}{V_f} - \frac{2}{3}\left[\frac{E_m}{E_f}(1 - 2v_f) - (1 - 2v_m)\right] \ln V_f \quad (2)$$

where V and v are the volume fraction and the Poisson's ratio of the matrix (subscript m) or of the reinforcement (subscript f), and ε_0 is the matrix uniaxial yield strain. This last parameter can be calculated through E_m and the matrix yield stress, (σ_y), in Table II. The experimental findings can be compared with the results of the calculations carried out according to Equations 1 and 2. The values of material properties reported in Table II were used in the calculation. Both the values of matrix CTE (α) in Table II were used obtaining a range for the critical temperature drop as a result. The critical ΔT for matrix deformation fluctuated between 285–331 °C or 558–648 °C, respectively when fibres or particles were considered as reinforcement. Because whiskers can be regarded as very short fibres (showing an aspect ratio different from 1), a behaviour between those of fibres and particles should be inferred. The forecasts obtained from the equations reported above agree with the experimental results. However, according to other equations found in the literature [38] the temperature drop required to cause a matrix stress exceeding its yield strength, which results in plastic flow, is much lower than that calculated here. It is to be underlined that all the equations assume that there is a perfect bond at the matrix–ceramic interface and that the matrix yield strength is the same as that of the unreinforced alloy. On the contrary, the strength of the interfacial bond can vary depending on the kind of composite, and the true yield strength of the composite matrix is greatly affected by the high density of dislocations.

3.2. Mechanical properties

Table III shows the variation of tensile properties, Brinell hardness and Charpy impact energy during thermal cycling for the unreinforced 6061 alloy and the composite 6061/SiC_w. The stress/strain curves of the materials in the T6 temper are compared with those characteristic of the samples cycled 2000 times between room temperature and 180 or 220 °C in Figs 2 and 3, for the unreinforced alloy and the composite material, respectively. The thermal cycling of 6061 alloy resulted in a decrease of yield strength and, in the case of the treatment carried out in the temperature range 25–220 °C, also in a decrease of hardness and in an increase of tensile elongation.

Specimens of 6061/SiC composite during thermal cycling underwent a more severe damage than the samples of the unreinforced alloy treated under the

TABLE II Properties of the composite constitutents

Material	E (GPa)	Poisson's ratio	Thermal expansion coefficient ($\times 10^{-6}$)	Yield strength (MPa)
6061	69 [43]	0.33 [41]	23.6 (20–100 °C) [41, 43] 26.7 (25–450 °C)[a]	276[a]
SiC_w	480 [43]	0.19 [43]	4.6 [42]	–

[a]Experimental result, this work.

TABLE III Mechanical properties of 6061 and 6061/SiC_w before and after thermal cycling: σ_y = yield strength, UTS = ultimate tensile strength, E = Young's modulus; Δl = elongation; HB = Brinell hardness; KV = Charpy impact energy.

Sample	σ_y (MPa)	UTS (MPa)	E (GPa)	Δl (%)	HB (kg mm^{-2})	KV (J)
6061 T6 temper	270	278	75	14.5	104	30
6061 500 cycles (25–180 °C)	266	274	81	15.0	103	32
6061 2000 cycles (25–180 °C)	265	278	81	13.8	101	42
6061 2000 cycles (25–220 °C)	229	274	74	16.2	87	52
6061/SiC T6 temper	395	546	114	3.5	119	5.7
6061/SiC 500 cycles (25–180 °C)	373	517	116	3.1	117	5.0
6061/SiC 2000 cycles (25–180 °C)	327	489	123	3.2	121	3.8
6061/SiC 2000 cycles (25–220 °C)	242	409	100	5.3	100	–

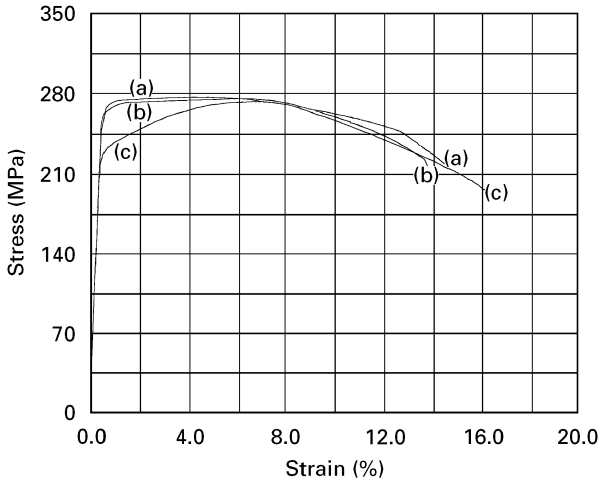

Figure 2 Stress–strain curves of unreinforced 6061 alloy (a) after T6 treatment, (b) after 2000 cycles between 25 and 180 °C, (c) after 2000 cycles between 25 and 220 °C.

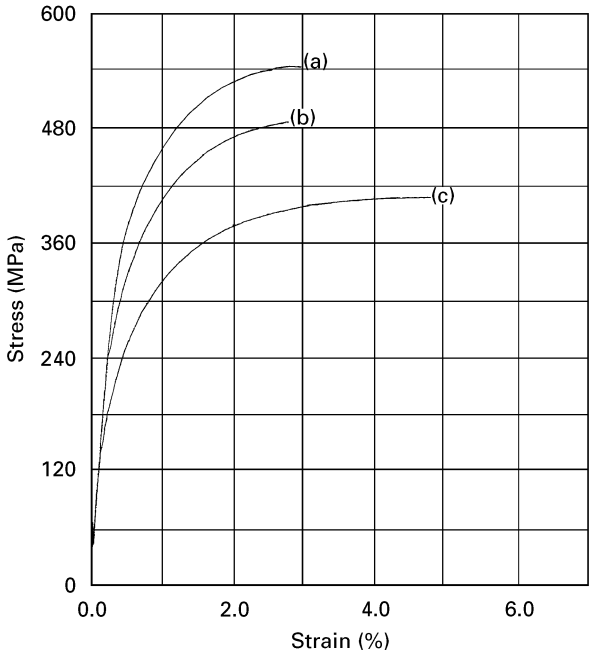

Figure 3 Stress–strain curves of 6061/SiC_w composite, (a) after T6 treatment, (b) after 2000 cycles between 25 and 180 °C, (c) after 2000 cycles between 25 and 220 °C.

same conditions. Table III and Fig. 3 show that thermal cycling caused the yield and the tensile strength of the composite to decrease, respectively, by 17% and 10% (for cycling between 25 and 180 °C) and by 39% and 25% (for cycling between 25 and 220 °C). The degradation of these properties progressed with the number of cycles and the temperature gap adopted in the treatment (Table III). Furthermore, a relevant increase of tensile specimen elongation (about 50%) and a hardness decrease of 16% were observed after composite cycling in the more severe conditions (2000 cycles in the temperature range 25–220 °C).

Figs 4–6 show, respectively, the fracture surfaces of 6061 tensile specimens after T6 treatment and after thermal cycling performed between room temperature and 180 or 220 °C. The samples of the unreinforced alloy always showed a typical ductile behaviour.

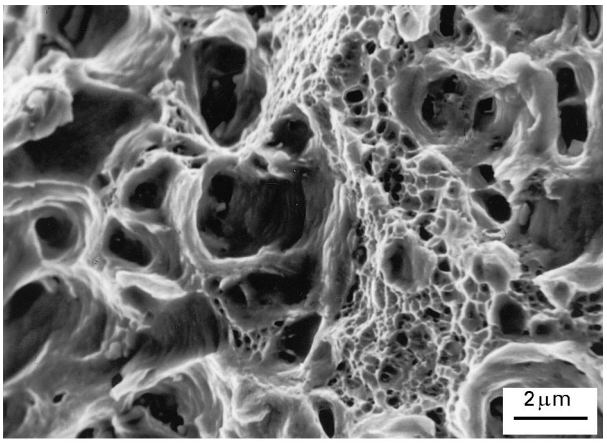

Figure 4 Fracture surface of tensile specimen of 6061 alloy in the T6 temper.

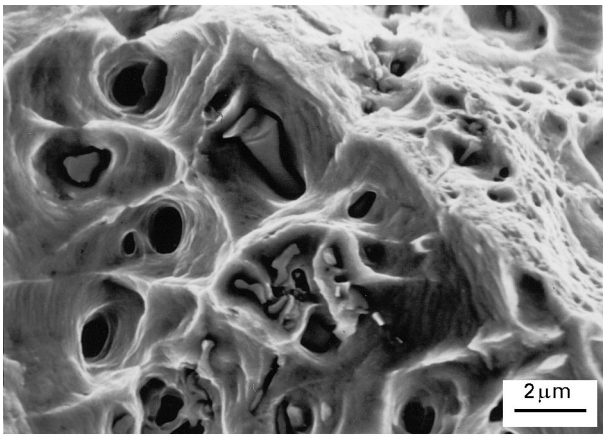

Figure 5 Fracture surface of tensile specimen of 6061 alloy after 2000 cycles up to 180 °C.

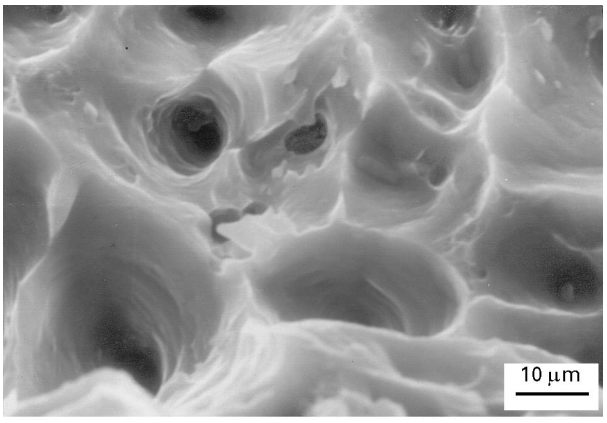

Figure 6 Fracture surface of tensile specimen of 6061 alloy after 2000 cycles up to 220 °C.

Uncycled 6061 and specimens that underwent 2000 cycles up to 180 °C exhibited very similar fracture surfaces. However, a prolonged thermal cycling between 25 and 220 °C determined the increase of void dimensions on the fracture surface (Fig. 6). Particles of precipitates, probably grown in the matrix during thermal exposure, were observed embedded inside the largest dimples (Fig. 5).

The fracture surfaces of the tensile specimens of the composite material after different thermal treatments

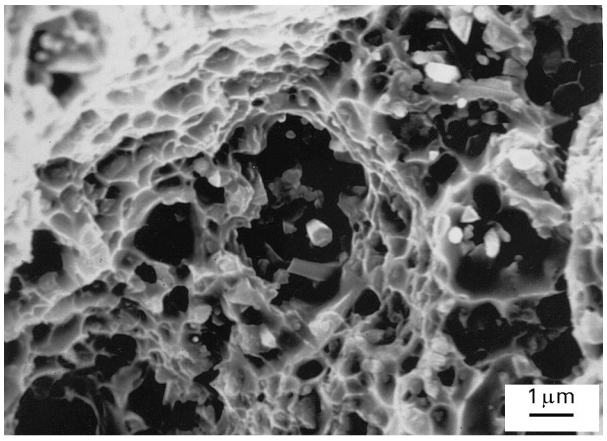

Figure 7 Fracture surface of tensile specimen of 6061/SiC composite in the T6 temper.

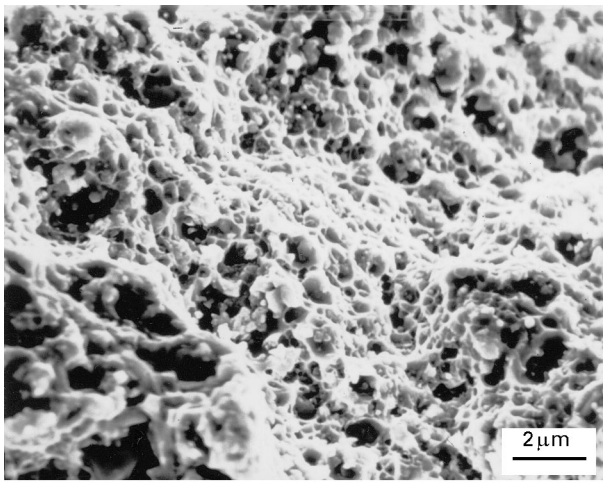

Figure 8 Fracture surface of tensile specimen of 6061/SiC composite after 2000 cycles up to 180 °C.

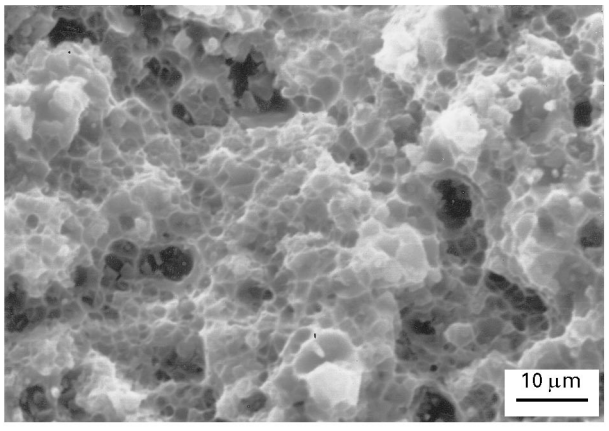

Figure 9 Fracture surface of tensile specimen of 6061/SiC composite after 2000 cycles up to 220 °C.

(T6, 2000 cycles up to 180 or 220 °C) are compared in Figs 7–9. These figures show that the fracture of the matrix occurred by a ductile mechanism, even though the composite material displayed a limited ductility on a macroscopic scale. Anyway, the dimples detected on the fracture surfaces of the composite were smaller than those observed for the unreinforced alloy. After 2000 cycles up to 220 °C the size of dimples was generally lower than 2 μm in the case of the composite and between 2 and 12 μm for the unreinforced alloy. Only small differences in the fracture morphology were found among composite samples in the T6 temper and those thermally cycled. The fracture surfaces of the composite tensile specimens were generally free of broken whiskers, even though debonded whiskers can be occasionally observed (Fig. 7). So, the failure mechanism of the composite involved whisker–matrix debonding and reinforcement pull-out. The ultrasound washing of the samples, which was carried out before the SEM observation, likely concurred to remove the reinforcement from the fracture surface.

The impact behaviour of 6061 alloy greatly differed from that of the composite: the load–time trace for the 6061 alloy exhibited general yielding (Fig. 10), while the trace for the composite showed brittle behaviour (Fig. 11). The value of fracture energy of the aluminium alloy was about one order of magnitude greater than that of the composite. Fig. 10 shows that the impact energy of the unreinforced alloy was enhanced by thermal cycling, probably because of sample overageing. The Charpy impact energy of composite specimens seems to be greatly affected by the presence of defects generated during the material processing and the subsequent thermal treatments. For this reason, a scatter in the results of the impact test was generally observed; this scattering was enhanced in the case of samples submitted to prolonged thermal cycling in severe conditions (for instance, specimens after 2000 cycles between 25 and 220 °C did not give significant Charpy results). However, the average values of Charpy impact energy displayed a clear trend following thermal cycling. Table III and Fig. 11 show that the toughness of the 6061/SiC composite greatly decreased during the thermal cycling. To investigate better the fracture nucleation mechanism, 6061/SiC T6 heat-treated and 6061/SiC thermally cycled composites were also tested according to fracture mechanics procedure. The experimental results ($K_{Ic} = 32\ MPa\ m^{1/2}$ for T6 samples and $K_{Ic} = 20\ MPa\ m^{1/2}$ for thermally cycled specimens – 2000 cycles between 25 and 220 °C) confirm the progressive toughness decrease of the composite with increasing thermal cycling severity.

The fractographies of T6 and thermally cycled samples evaluated at the tip of precracks are compared in

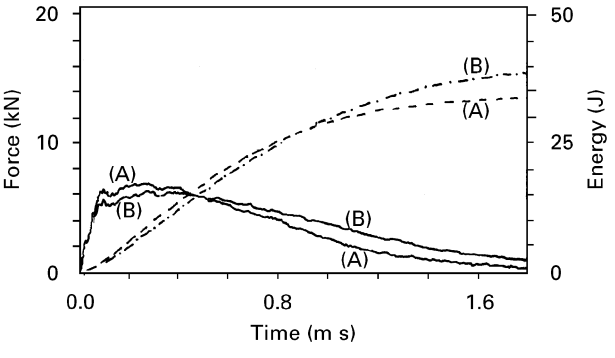

Figure 10 Charpy curves for unreinforced 6061 alloy: (A) T6 temper; (B) after 2000 cycles between 25 and 180 °C. (——) Force, (– – –) energy.

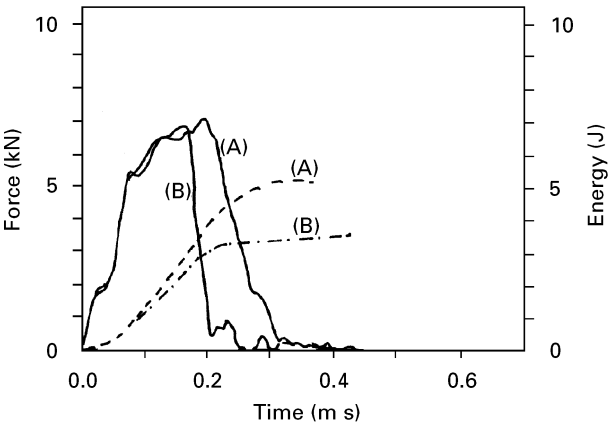

Figure 11 Charpy curves for 6061/SiC composite: (A) T6 temper; (B) after 2000 cycles between 25 and 180 °C. (——) Force, (– – –) energy.

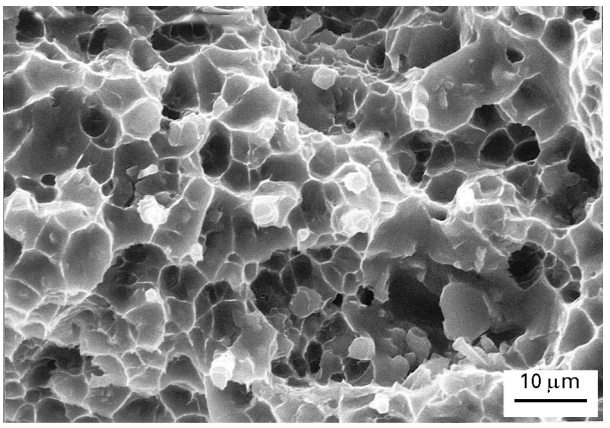

Figure 14 6061/SiC composite after 2000 cycles up to 220 °C: whiskers on the fracture surface of SENB specimen.

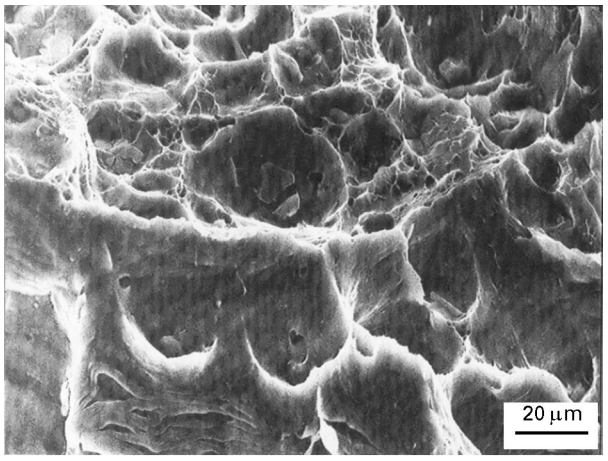

Figure 12 6061/SiC composite in the T6 temper: fracture surface of SENB specimen.

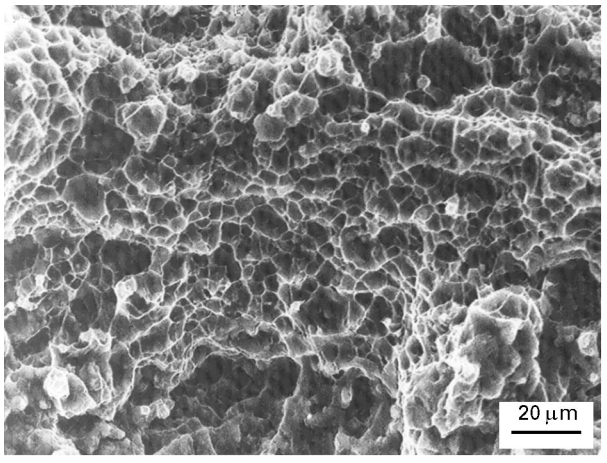

Figure 13 6061/SiC composite after 2000 cycles up to 220 °C: fracture surface of SENB specimen.

Figs 12 and 13. A stretch zone varying between 5 and 50 μm, and a subsequent ductile zone characterized by microvoids nucleated around whiskers and matrix precipitates, are the typical modes of fracture for 6061/SiC T6 composite. The largest voids are localized around the matrix precipitates which, if placed in a highly stressed zone (the crack tip) and in the presence of a sufficiently high dimension of the particles, can break down (Fig. 12).

No stretch zones were observed in the case of 6061/SiC cycled composite (2000 cycles 25–220 °C). Although the thermal fatigue does not affect the fracture behaviour (the ductile mechanism is always present) a significant difference is evident in the dimension of the microvoids which, after thermal cycles, are clearly smaller. Another difference appears when comparing the fracture surfaces of tensile and fracture mechanics composite samples. In fact, for the latter, it is easier to observe debonded whiskers on the fracture surface (Fig. 14). This phenomenon can be attributed to the change in fibre orientation with respect to the applied load: longitudinal for tensile samples and transverse for the SENB (single-edge notched bend) specimens.

Unreinforced 6061 and 6061/SiC composite underwent damaging processes with different mechanisms during the course of thermal cycling, as evinced by the modification of mechanical properties reported in Table III. Thermal cycling involves the exposure of the investigated materials at high temperatures (180 or 220 °C) for long periods (at least 200 h after 2000 cycles). Because of standing at high temperature, the 6061 alloy and the aluminium metal matrix of the composite achieve an overageing condition, which entails the increase of both the size of hardening precipitates and the interspaces between these particles. Overageing generally causes an increase of ductility, that is, a degradation of yield strength and hardness: actually this behaviour was observed during cycling of unreinforced 6061 alloy. Furthermore, the increased ductility of 6061 samples cycled between room temperature and 220 °C resulted in an enhanced elongation under tensile load, in an enlargement of dimples on the fracture surface, and in an increase of Charpy impact resistance. However, a complete overageing of the unreinforced alloy should occur after 2000 cycles between 25 and 180 °C as well as after the analogous treatment performed between 25 and 220 °C. Thus, overageing cannot explain the different values of yield strength and hardness measured for the 6061 samples cycled in different conditions (maximum temperature of 180 or 220 °C). It should be pointed out that during

thermal cycling of aluminium alloy, other complex phenomena occur. Internal stresses arise from the interior-to-surface temperature gradients; these stresses can be relieved, for instance through dislocation formation. The full annealing of 6061 is accomplished by heating at 415 °C for about 3 h; however, annealing can occur also as a consequence of prolonged thermal exposure at lower temperatures. As the cycling treatment involved long periods at 180 or 220 °C, an incomplete softening of the aluminium alloy could result from stress relief, changes in dislocation density and arrangement, and partial recrystallization. In addition, thermal cycling was generally found to cause the coalescence of pores, as will be discussed in the next section.

The metal matrix of the composite following thermal cycling should undergo overageing and recrystallization in the same manner as the unreinforced alloy. However, yield strength decreased much more during the treatment of the composite material than during the analogous treatment of 6061 alloy. Tensile specimens of 6061/SiC showed, after cycling, an increase of elongation (up to 50%) which was not justified by the morphology of the fracture surface. In addition, thermal cycling greatly lowered the tensile strength of the composite, while this property was not affected by the treatment in the case of the unreinforced alloy. Finally, the Charpy impact resistance of 6061 alloy and of 6061/SiC composite changed in the opposite way during the thermal cycling: the first material became more ductile and the second showed a sharp increase of brittleness. The variation found in K_{Ic} values confirms the decrease of fracture toughness of thermally cycled composite materials.

The different behaviour of the two materials under investigation could be due to the large thermal stresses that are generated during cycling in the composite as a consequence of the great difference in the thermal expansion coefficients of silicon carbide and aluminium metal matrix. These stresses can generate defects in the microstructure of the composite, and defects are likely to dominate the fracture mechanism.

3.3. Porosity

Scanning electron microscopy and mercury intrusion porosimetry showed that both unreinforced alloy and 6061/SiC composite in the T6 temper had about 0.5% porosity. The pore size was generally lower than 1 μm, but larger voids were occasionally observed at the matrix/reinforcement interface in the case of the composite. Thermal cycling resulted in a coalescence of voids: this phenomenon occurred in the unreinforced alloy (Fig. 15) and in the composite as well (Fig. 16). On the other hand, density measurements (Table I) and porosimetry concurred to demonstrate that the percentage of voids did not increase during thermal cycling. Coalescence of porosity was more marked inside the composite specimens than for unreinforced 6061 (Table IV). According to mercury intrusion porosimetry, only in the case of the composite material did a significant number of voids grow above 1 μm. Pores of 1 μm diameter or more were also observed by SEM in the metallographic sections of unreinforced 6061 (Fig. 15), but these voids were a negligible part of the cumulative sample porosity.

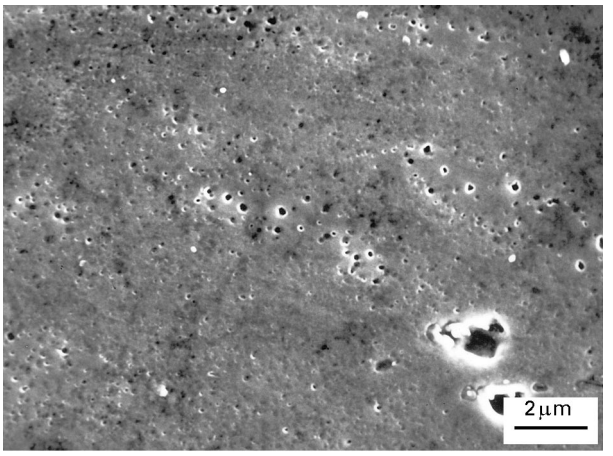

Figure 15 Porosity in unreinforced 6061 after 2000 cycles between 25 and 180 °C.

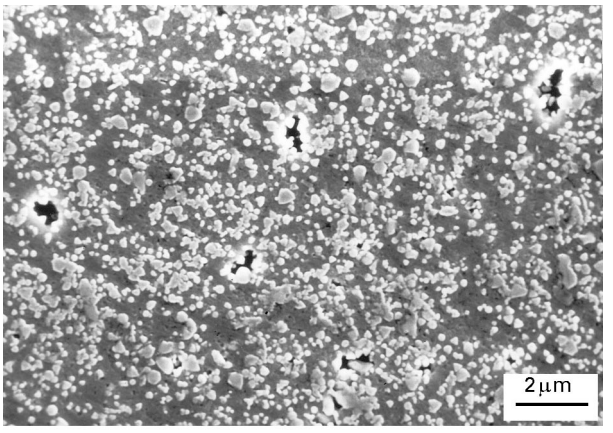

Figure 16 Porosity in 6061/SiC composite after 2000 cycles between 25 and 180 °C.

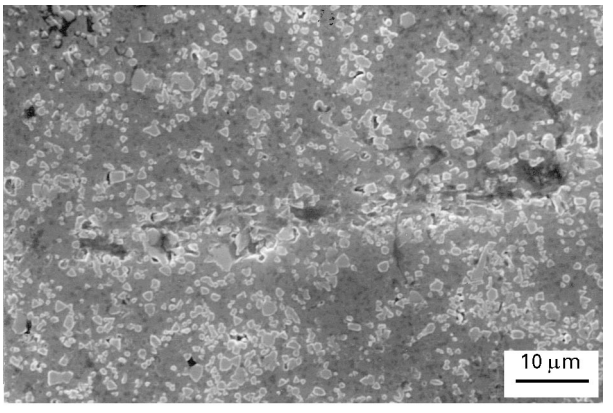

Figure 17 Reorganization of porosity to form cracks in 6061/SiC after 2000 cycles between 25 and 220 °C.

However, these two materials showed a different behaviour, chiefly because only in the case of the composite did the voids progressively reorganize. Following this reorganization, crack formation started (Fig. 17).

TABLE IV Pore-size distribution in 6061 unreinforced alloy and 6061/SiC composite before and after thermal cycling

Sample	Cumulative porosity in the dimensional range (%)			
	1–6 μm	0.1–1 μm	0.01–0.1 μm	0.03–0.01 μm
6061 T6 temper	–	–	2	98
6061 2000 cycles (25–180 °C)	–	2	41	56
6061 2000 cycles (25–220 °C)	–	3	58	39
6061/SiC T6 temper	–	–	58	42
6061/SiC 2000 cycles (25–180 °C)	5	–	63	32
6061/SiC 2000 cycles (25–220 °C)	9	2	47	42

TABLE V Thermal expansion coefficient, α, of unreinforced 6061 alloy and 6061/SiC composite measured in the temperature range between 25 and 450 °C

Material	Thermal expansion coefficient, α ($\times 10^{-6}$) for treatment conditions		
	T6	2000 cycles (25–220 °C)	20 cycles (25–500 °C)
6061 alloy	26.70	27.05	27.05
6061/SiC	13.55	14.79	17.66

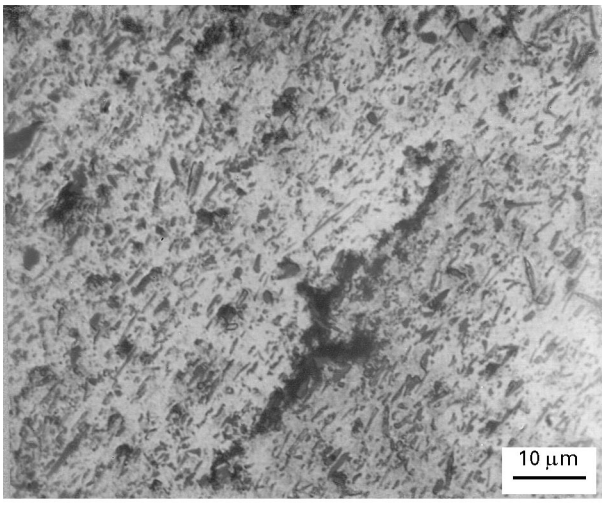

Figure 18 Crack formation in 6061/SiC after 20 cycles between 25 and 500 °C.

3.4. Thermal expansion

The coefficients of thermal expansion (CTE) measured by dilatometry between 25 and 450 °C are reported in Table V. The coefficient of thermal expansion of 6061 unreinforced alloy did not change after thermal cycling: only a variation of about 1.3% resulted from severe thermal treatments. On the contrary, the CTE of the composite material increased by 9% after 2000 cycles between 25 and 220 °C and by 30% after 20 cycles between 25 and 500 °C. Large cracks were observed by an optical microscope on the section of composite samples cycled under the latter conditions (Fig. 18). The CTE of a composite only depends on the thermal expansion of the components of the material and on the interfacial bonds between matrix and reinforcement. According to the literature [39, 40], no reaction can occur between silicon carbide and aluminium below 700 °C; furthermore, in the case of 6061 alloy this reaction is hindered by the presence of silicon in the metal matrix. In agreement with the literature findings, SEM observation of our composite samples did not show reaction products at the matrix/reinforcement interface, but only void formation. So, the variation after treatment of the composite expansion coefficient cannot be attributed to the growth of a reaction layer at the SiC/matrix interface. Thus, interfacial phenomena of debonding are responsible for the thermal expansion increase of composite specimens.

4. Conclusion

During thermal cycling, a 6061 unreinforced alloy behaved in a different way to its composite containing whiskers of silicon carbide. These two materials were cycled in ranges of temperatures (25–180 °C and 25–220 °C) that the composite is likely to experience in service.

The internal stresses, generated during cycling because of both the temperature gradients inside the specimens and the different thermal expansion of SiC and matrix, were not strong enough to cause matrix plastic flow: consequently, the two materials under investigation showed a good dimensional stability. However, during the treatment the materials underwent modifications of their microstructures which were detrimental to the mechanical properties. The degree of damage increased with the number of cycles and the maximum temperature reached in the course of the treatment.

The changes in the microstructural features that occurred in 6061 alloy were chiefly due to overageing and partial annealing. The treated 6061 alloy showed an increase of ductility: yield strength and hardness were lowered, while Charpy impact energy, elongation and dimension of voids on the fracture surface, were enhanced.

The metal matrix of the composite suffered overageing and annealing like the unreinforced alloy. However, following the cycling of the composite material, yield strength, tensile strength, fracture toughness and elongation changed so much that a further damaging mechanism should be considered.

Significant coalescence of porosity, involving the growth of large cavities at the interfaces between the

reinforcement and the matrix, and a reorganization of voids with the formation of cracks were observed in the composite samples.

The characteristics of the fracture surface of the composite demonstrated that whiskers are prone to undergo debonding and pull-out. A further weakening of the interfacial SiC/matrix bond occurred during thermal cycling, as was shown by the increase of the composite expansion coefficient. The composite CTE became progressively nearer to that of the unreinforced alloy following thermal cycling.

The failure mode of the cycled composite was dominated by the presence of defects: voids, cracks, debonded whiskers. In fact, composite thermal cycling resulted in a sharp decrease of tensile strength, Charpy impact energy and fracture toughness. The morphology of the fracture surface of the composite is similar for the T6 temper and thermally cycled tensile specimens: a ductile matrix mechanism is always present. On the other hand, marked differences were observed in terms of stretch zone extension, dimple dimensions and whisker pull-out phenomenon for the fracture mechanics samples; there differences are measurable differences in terms of progressive toughness decreasing with increasing thermal cycling severity.

References

1. M. VOGELSANG, R. J. ARSENAULT and R. M. FISHER, *Metall. Trans.* **17A** (1986) 379.
2. Y. FLOM and R. J. ARSENAULT, *J. Metals* **38** (1986) 31.
3. N. SHI, R. J. ARSENAULT., A. D. KRAWITZ and L. F. SMITH, *Metall. Trans.* **24A** (1993) 187.
4. A. WEILAND and T. JOHANNESSON, *Mater. Sci. Eng.* **A190** (1995) 131.
5. F. S. SHIEU and S. L. SASS, *Acta Metall. Mater.* **39** (1991) 539.
6. F. REZAI-ARIA, T. LICHTI and G. GAGNON, *Scripta Metall. Mater.* **28** (1993) 587.
7. S. IG HONG, G. T. GRAY III and K. S. VECCHIO, *Mater. Sci. Eng.* **A171** (1993) 181.
8. S. M. PICKARD and B. DERBY, *Acta Metall. Mater.* **38** (1990) 2537.
9. M. TAYA and T. MORI, in "Thermomechanical Coupling in Solids", edited by H. D. Bui and Q. S. Ngueyn (Elsevier Science, North-Holland, IUTAM, 1987) pp. 147–62.
10. G. GARMONG, *Metall. Trans.* **5A** (1974) 2183.
11. *Idem*, *ibid.* **5A** (1974) 2199.
12. S. YODA, N. KURIHARA, K. WAKASHIMA and S. UMEKAWA, *ibid.* **9A** (1978) 1229.
13. S. V. NAIR and H. G. KIM, *Scripta Metall. Mater.* **25** (1991) 2359.
14. E. U. LEE, *Metall. Trans.* **23A** (1992) 2205.
15. H. ZHANG, G. S. DAEHN and R. H. WAGONER, *Scripta Metall. Mater.* **25** (1991) 2285.
16. W. D. ARMSTRONG, PhD Thesis (1991); (U.M.I. Dissertation Services, Bell and Howell Company, Ann Arbor, MI).
17. M. Y. WU and O. D. SHERBY, *Scripta Metall.* **18** (1984) 773.
18. B. DERBY, *ibid.* **19** (1985) 703.
19. J. C. LE FLOUR and R. LOCICERO, *ibid.* **21** (1987) 1071.
20. G. S. DAEHN and T. OYAMA, *ibid.* **22** (1988) 1097.
21. F. BONOLLO, L. CESCHINI, G. L. GARAGNANI, F. PERSIANI and A. ZAMBON, *Metall. Ital.* **84** (1992) 975.
22. G. S. DAEHN, P. M. ANDERSON and H. ZHANG, *Scripta Metall. Mater.* **25** (1991) 2279.
23. G. NEITE and S. MIELKE, *Mater. Sci. Eng.* **A148** (1991) 85.
24. R. A. MACKAY, *Scripta Metall. Mater.* **24** (1990) 167.
25. W. C. REVELOS and P. R. SMITH, *Metall. Trans.* **23A** (1992) 587.
26. S. M. RUSS, *ibid.* **21A** (1990) 1595.
27. Y. H. PARK and H. MARCUS, in "Mechanical Behaviour of Metal Matrix Composites", edited by J. E. Hack and M. F. Amateau, (The Metallurgical Society of AIME, Warrendale, PA, 1983) pp. 65–75.
28. S. H. THOMIN, P. A. NOEL and D. C. DUNARD, *Metall. Mater. Trans.* **26A** (1995) 883.
29. A. K. MISRA, *Scripta Metall. Mater.* **28** (1993) 1189.
30. A. K. MISRA, R. R. BOWMAN, *Mater. Sci. Eng.* **A196** (1995) 197.
31. S. YODA, R. TAKAHASHI, K. WAKASHIMA and S. UMEKAWA, *Metall. Trans.* **10A** (1979) 1796.
32. W. G. PATTERSON and M. TAYA, in "Proceedings of ICCM5", edited by W. C. Harrigan, J. Strike and A. K. Dhingra, (TMS-AIME, Warrendale, PA, 1985) pp. 53–65.
33. C. M. WARWICK and T. W. CLYNE, in "Proceedings Institution Mechanical Engineers Conference, Vol. 3, Fibre Reinforced Composites", (Mechanical Engineering Publications, Bury St Edmunds, UK) pp. 169–77.
34. I. W. HALL and W. G. PATTERSON, *Scripta Metall. Mater.* **25** (1991) 805.
35. C. S. LIN, in "Proceedings of the 38th SAMPE Symposium", "Advanced Materials: Performance Through Technology Insertion" Vol. 38-I (Society for the Advancement of Materials and Processing, Covina, CA, 1993) pp. 98–104.
36. T. J. REINHART, (ed.), "Engineered Materials Handbook", Vol. 1 (ASM International, Metal Park, OH, 1987) p. 890.
37. C. BADINI, F. MARINO and A. TOMASI, *J. Mater. Sci.* **26** (1991) 6279.
38. H. M. LEDBETTER and M. W. AUSTIN, *Mater. Sci. Eng.* **89** (1987) 53.
39. T. ISEKI, T. KAMEDA and T. MARUYAMA, *J. Mater. Sci.* **19** (1984) 1692.
40. J. C. VIALA, P. FORTIER and J. BOUIX, *ibid.* **25** (1990) 1842.
41. "ASM Handbook" 9th Edn Vol. 2 (ASM, Metals Park, OH 1979) edited by W. H. Cubberley *et al.* pp. 116–7.
42. E. A. BRANDES and C. B. BROOK (eds), "Smithells Metals Reference Book", 7th Edn (Butterworth–Heinemann, Oxford, 1992) p. 27–2.
43. C. T. LYNCH (ed.), "Handbook of Materials Science", (CRC Press, Boca Raton, FL, 1989) p. 318.

Received 19 April
and accepted 12 August 1996